Annals of Clinical and Translational Neurology

RESEARCH ARTICLE OPEN ACCESS

Value of MRI Outcomes for Preventive and Early-Stage Trials in Spinocerebellar Ataxias 1 and 3

Thiago J. R. Rezende[1] | Emilien Petit[2] | Young Woo Park[3,4,5] | Sophie Tezenas du Montcel[2] | James M. Joers[3] | Jonathan M. DuBois[6] | H. Moore Arnold[6] | Michal Povazan[7] | Ipek Özdemir[7] | Guita Banan[8] | Romain Valabregue[2] | Philipp Ehses[9] | Jennifer Faber[9,10,11] | Chiadi U. Onyike[12] | Peter B. Barker[7] | Jeremy D. Schmahmann[13] | Eva-Maria Ratai[14] | Sub H. Subramony[8] | Thomas H. Mareci[8] | Khalaf O. Bushara[3] | Henry Paulson[15] | Thomas Klockgether[9,10] | Alexandra Durr[2] | Tetsuo Ashizawa[16] | Christophe Lenglet[3] | Gülin Öz[3] | READISCA Investigators

[1]Department of Neurology, School of Medical Sciences, University of Campinas, Campinas, Brazil | [2]Inserm, INRIA, CNRS, APHP, Paris Brain Institute, Sorbonne Université, Paris, France | [3]Department of Radiology, Center for Magnetic Resonance Research, University of Minnesota, Minneapolis, Minnesota, USA | [4]Henry M. Jackson Foundation for the Advancement of Military Medicine, Inc, Bethesda, Maryland, USA | [5]Department of Radiology, Uniformed Services University of the Health Sciences, Bethesda, Maryland, USA | [6]Biogen, Cambridge, Massachusetts, USA | [7]Department of Radiology and Radiological Sciences, Johns Hopkins University School of Medicine, Baltimore, Maryland, USA | [8]Norman Fixel Institute for Neurological Disorders, College of Medicine, University of Florida, Gainesville, Florida, USA | [9]German Center for Neurodegenerative Diseases (DZNE), Bonn, Germany | [10]Department of Neurology, University Hospital Bonn, Bonn, Germany | [11]Department of Neuroradiology, University Hospital Bonn, Bonn, Germany | [12]Department of Psychiatry and Behavioral Sciences, Johns Hopkins University School of Medicine, Baltimore, Maryland, USA | [13]Ataxia Center, Laboratory for Neuroanatomy and Cerebellar Neurobiology, Department of Neurology, Massachusetts General Hospital and Harvard Medical School, Boston, Massachusetts, USA | [14]Department of Radiology, A. A. Martinos Center for Biomedical Imaging, Massachusetts General Hospital, Harvard Medical School, Boston, Massachusetts, USA | [15]Department of Neurology, University of Michigan, Ann Arbor, Michigan, USA | [16]Stanley H. Appel Department of Neurology, Houston Methodist Research Institute and Weill Cornell Medicine, Houston, Texas, USA

Correspondence: Gülin Öz (gulin@cmrr.umn.edu)

Received: 16 December 2025 | **Accepted:** 3 January 2026

Keywords: longitudinal | MRI | spinocerebellar ataxia

ABSTRACT

Objective: To examine the value of MRI outcomes as endpoints for preventive and early-stage trials of two polyglutamine spinocerebellar ataxias (SCAs).

Methods: A cohort of 100 participants (23 SCA1, 63 SCA3, median Scale for the Assessment and Rating of Ataxia (SARA) score = 5, 42% preataxic, and 14 gene-negative controls) was scanned at 3T up to 6 times (median follow-up 3 years) in the READISCA study. Structural, microstructural, and neurochemical outcomes were assessed for sensitivity to change. Associations between change in MR and clinical and patient-reported outcomes were evaluated. Sample sizes were estimated for preventive trials (at preataxic stage) and early-stage trials using the most sensitive outcomes.

Results: Infratentorial volumes, middle cerebellar peduncle (MCP) diffusivities and select neurochemical outcomes were more sensitive to change than SARA in both SCAs with moderate-to-high effect sizes (Cohen's $d \geq 0.5$). The pons volume was the most sensitive outcome at both preataxic ($d = 1.09$) and ataxic ($d = 1.48$) stages. The most sensitive MR measures overlapped between genotypes, except that SCA1 showed faster progression in the cerebellum and SCA3 in the pons. Changes in MCP diffusivities and pontine neurochemical measures were associated with changes in SARA and FARS-ADL ($|r| = 0.28–0.47$).

Thiago J. R. Rezende and Emilien Petit contributed equally to this article.

Dr. Park contributed to the work while at the University of Minnesota.

Interpretation: The estimated sample sizes to detect a 50% reduction in progression with 80% power using the pons volume as primary outcome measure indicate the feasibility of preventive trials ($n = 73$ per arm in a 1-year trial) in common SCAs and predict a 6-fold reduction in required sample sizes relative to SARA in early interventional trials. These findings support the use of MRI endpoints in early-stage SCA trials.

1 | Introduction

Polyglutamine spinocerebellar ataxias (SCAs) are hereditary neurodegenerative diseases caused by CAG repeat expansions and present with progressive cerebellar ataxia, fine motor coordination deficits and speech impairment [1]. To date, there are no disease-modifying treatments for SCAs, but a growing number of treatments, including gene silencing approaches, are in the therapeutic pipeline [2]. Early interventions prior to substantial neuronal loss may prevent the progression of pathology and even reverse neuronal dysfunction in SCAs [3]. However, clinical outcome assessments (COAs), such as the Scale for the Assessment and Rating of Ataxia (SARA) [4], are not sensitive to change during the preataxic disease stage [2] hampering their use as endpoints for preventive SCA trials. In addition, trial designs that are used in more common [5] and faster progressing [6] neurodegenerative diseases to assess if interventions delay the onset of clinically manifest disease are prohibitive in the rare, slowly progressing SCAs.

Quantitative MRI outcomes may facilitate very early-stage SCA trials since they detect cerebral changes that precede motor symptoms cross-sectionally [7, 8]. Furthermore, the potential for MRI outcomes to track early-stage pathology progression was demonstrated in single-site studies [9–13] and in a recent multisite SCA3 project [14]. Importantly, clinical trials increasingly utilize neuroimaging outcomes [15, 16]. With the possibility of preventive trials in SCAs, where CAG expansion carriers can be identified before onset of cerebellar signs, there remains a great need to assess the trial readiness of multimodal MRI outcomes in the multisite setting at very early disease stages.

READISCA [7, 17, 18] is a multisite longitudinal study that built a trial-ready cohort of preataxic and early-stage carriers of SCA mutations and matched gene-negative individuals to identify clinical and imaging outcomes for early-stage trials. Enrollment focused on SCA1 as the fastest progressing and SCA3 as the most common dominantly inherited ataxia. The project demonstrated the exquisite sensitivity of multimodal MRI to cross-sectionally detect volumetric, microstructural, and neurochemical abnormalities in preataxic and early SCA1 and SCA3 [7]. Furthermore, select MR measures captured disease progression over 6 months in a subset of the cohort [7, 17]. Here we present longitudinal structural, diffusion MRI, and MR spectroscopy (MRS) findings in the READISCA cohort that was scanned annually up to 6 times at 4 US and 2 European sites. We identified the MR outcomes that are most sensitive to change at preataxic and early-stage, investigated if the sensitive MR measures differed between SCA genotypes, and evaluated their associations with COA changes, including patient-reported outcome measures (PROMs).

2 | Methods

2.1 | Study Design and Participants

In this prospective cohort study, 100 participants from the READISCA (https://clinicaltrials.gov/ct2/show/NCT03487367) imaging cohort [7] were imaged and assessed with a comprehensive clinical battery [18] annually from 2018 to 2023 (Table 1). A subset ($N = 44$) was also scanned 6 months after baseline [17], resulting in up to 6 imaging visits in this group. The sample size for follow-up visits was determined by participants' willingness to return during the COVID-19 pandemic (Figure 1, Tables S1–S4). Participants were enrolled at 16 sites and scanned at six sites [7, 17]. Early-stage SCA1 or SCA3 expansion carriers (SARA < 10) and matched gene-negative controls were enrolled using inclusion/exclusion criteria described previously [7]. As is standard in the field, a SARA threshold of 3 (out of a maximum score of 40 indicating severe ataxia) was used as indicative of manifest ataxia; expansion carriers with SARA < 3 were classified as preataxic [7, 19].

The study was approved by the Institutional Review Board at each site and informed consent was obtained. One individual was excluded from the analysis due to incidental findings in structural brain MRI that were unrelated to SCA.

2.2 | Clinical Outcome Assessments (COAs)

Ataxia severity was assessed using the SARA score at all visits. SARA is a standardized composite clinical scale with demonstrated construct validity, internal consistency, and inter-rater reliability [4]. The SARA score quantifies ataxia severity through assessments of gait, stance, sitting balance, speech, and coordination tasks, including finger-chase, nose-finger, fast alternating hand movements, and heel-shin tests [4]. As previously described in the imaging and clinical baseline studies [7, 18], annual visits also included the Inventory of Non-Ataxia Signs (INAS), Composite Cerebellar Function Score (CCFS), Cerebellar Cognitive Affective Syndrome (CCAS) scale, Fatigue Severity Scale (FSS), Friedreich Ataxia Rating Scale—Activities of Daily Living (FARS-ADL), Patient Health Questionnarie-9 (PHQ-9) and the European Quality of life-5 Dimensions index (EQ-5D). Ataxic participants reported their age at ataxia onset (Table 1). The time from ataxia onset at baseline was estimated using the CAG repeat length for all mutation carriers, as described previously [7, 17, 18]. Plasma neurofilament light chain (NfL) was measured at each annual visit as previously described [18].

TABLE 1 | Cohort characteristics at baseline, data availability at follow-up and SARA evolution during follow-up.

Variable	Control ($N=14$)	SCA1 ($N=23$)	SCA3 ($N=63$)	p[a]	Preataxic ($N=36$)	Ataxic ($N=50$)	p[b]
Age (IQR), years	45.5 (38.2; 53.5)	41 (33; 49.5)	42 (36; 50.5)	0.67	37 (32.7; 42.5)	47.5 (40.2; 53)	0.002
Sex (female %)	6 (42.9%)	16 (69.6%)	36 (57.1%)	0.27	25 (69.4%)	27 (54%)	0.17
Handedness (right %)	12 (92.3%) $n=13$	20 (87%)	54 (85.7%)	0.81	31 (86.1%)	43 (86%)	0.82
CAG repeat length (IQR), short allele	NA	29.5 (29; 30) $n=22$	23 (20; 24) $n=57$	<0.0001	27 (23; 28.5) $n=35$	23 (21; 27.5) $n=44$	0.29
CAG repeat length (IQR), long allele	NA	44 (42; 45.8) $n=22$	71 (69; 73) $n=61$	<0.0001	69 (45.5; 71) $n=35$	70.5 (57.2; 73) $n=48$	0.41
Plasma NfL, pg/mL	3.9 (3.1; 5.5) $n=10$	17.5 (13.2; 22) $n=14$	19 (13.6; 23.4) $n=48$	<0.0001	13.8 (10.5; 17.8) $n=27$	21.9 (17.2; 25.5) $n=35$	<0.001
Estimated time from ataxia onset (IQR), years[c]	NA	−0.6 (−6.3; 5.4) $n=22$	5.9 (−0.9; 10.8) $n=61$	0.047	−3.0 (−7.8; 1.5) $n=35$	9.4 (4.6; 12.1) $n=48$	<0.001
SARA at baseline (IQR)	0 (0; 0.8)	4.5 (1.2; 8.8)	4.5 (2; 7.2)	0.0002	1 (0; 2)	7.2 (5.5; 8.5)	<0.001
SARA change (IQR)	−0.1 (−0.1; −0.1)	0.5 (0.1; 1.2)	0.5 (0; 1)	0.0011	−0.1 (−0.1; 0.1)	0.9 (0.6; 1.5)	<0.001
Follow-up duration (IQR), years	3.1 (2.7; 4.1)	2.6 (2.1; 3.4)	2.6 (2.0; 3.4)	0.40	2.8 (2.0; 3.9)	2.6 (2.0; 3.3)	0.30
Time between visits (IQR), years	1.0 (0.9; 1.5)	0.9 (0.8; 1.1)	1.0 (0.9; 1.1)	0.35	1.0 (0.9; 1.1)	1.0 (0.9; 1.1)	0.69
Number of MRI scans (IQR)	3 (3; 5)	4 (3; 4.5)	3 (3; 4)	0.40	3 (3; 4.2)	3 (3; 4)	0.58
Number of clinical assessments (IQR)	5 (3; 5)	4 (3; 5)	4 (3; 5)	0.63	4 (3; 5)	4 (3; 5)	0.61
Number of converters (%)	0 (0%)	3 (13%)	8 (12.7%)	0.36	11 (30.6%)	0 (0%)	<0.001

Note: For categorical variables frequencies are provided using percentages, and for quantitative variables median and interquartile range (Q1; Q3) are provided; n is provided when values are reported by a subset of the cohort or are missing.

[a]ANOVA p-values for comparison among SCA1, SCA3, and control groups.

[b]ANOVA p-values for comparison among preataxic, ataxic, and control groups.

[c]Estimated time from onset was calculated for all mutation carriers using the CAG repeat length.

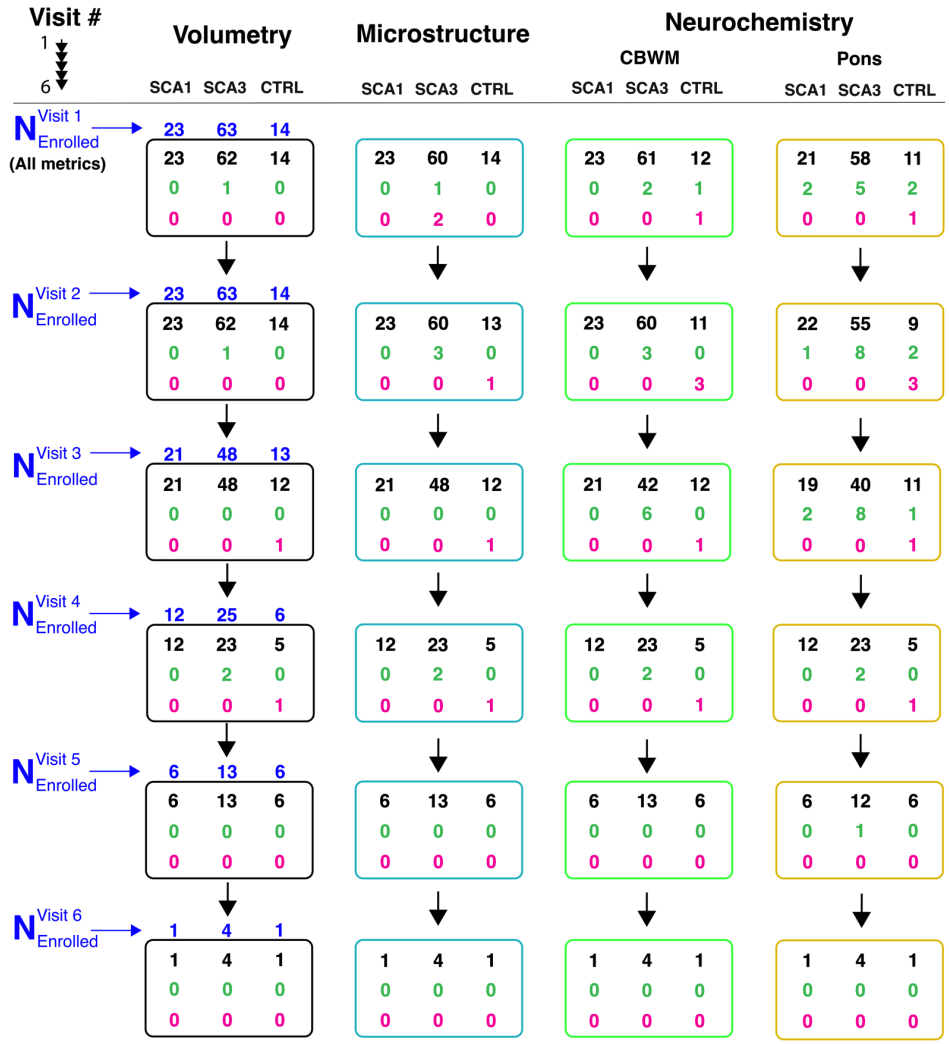

FIGURE 1 | Sample sizes for each magnetic resonance modality (structural, diffusion MRI and MR spectroscopy with two regions of interest, cerebellar white matter and pons) at the 6 study visits. Missing data (pink) and data excluded (green) based on incidental findings and quality control criteria are indicated.

2.3 | MR Imaging

2.3.1 | Data Acquisition

MRI scans were performed on 3T Siemens systems (five Prisma and one Skyra) running Syngo MR E11, utilizing body coil transmission and a 32- or 64-channel receiver array. Structural and diffusion MRI sequences were harmonized with the Human Connectome Project (HCP) lifespan protocol [20] and key parameters included:

- 3-dimensional (3D) T1-weighted magnetization-prepared rapid acquisition gradient echo: acquired in the sagittal plane, 0.8 mm^3 isotropic resolution, Repetition Time (TR) = 2400 ms, echo time (TE) = 2.2 ms, inversion time = 1000 ms, flip angle 8°, generalized autocalibrating partially parallel acquisition (GRAPPA) = 2.
- 3D T2-weighted SPACE (sampling perfection with application-optimized contrasts using different flip angle evolution): acquired in the sagittal plane, 0.8 mm^3 isotropic, TR/TE = 3200/563 ms, GRAPPA 2.
- Diffusion MRI: Acquired with multiband acceleration (factor 4) and reverse phase encoding. Prisma: 1.5 mm^3 isotropic, TR/TE = 3230/89.2 ms, b values = 1500/3000 s/mm^2; Skyra: 1.7 mm^3 isotropic, TR/TE = 3390/103.2 ms, b value = 1000/2000 s/mm^2. Both scanners used a matched q-space scheme, acquired in the axial plane with 92 slices to guarantee full coverage of the cerebellum.

MRS data were acquired from the pons and cerebellar white matter using an automated and harmonized semi-adiabatic localization by adiabatic selective refocusing (sLASER) protocol [21] (TR/TE = 3000/30 ms, 80 transients) with integrated B0 and B1 calibration [22]. Volumes of interest (VOIs) were automatically prescribed in the pons (16 × 16 × 16 mm^3) and cerebellar white matter (17 × 17 × 17 mm^3) using the AutoVOI software [23], except for one site due to network issues. Unsuppressed water spectra were collected for quantification and eddy current correction [24].

2.4 | Quality Control (QC), Preprocessing and Data Availability

Participants from the READISCA imaging cohort with at least two timepoints were included in this study, including eight additional participants enrolled after the baseline MRI findings were published [7].

All DICOM files were anonymized with DicomBrowser [25] and structural images were defaced using Face Masking [26] prior to upload onto a centralized Flywheel (https://flywheel.io/) database housed at the University of Minnesota. A standardized Docker container enabled consistent de-identification and data transfer across sites.

MR image analysis was conducted blinded to participant diagnosis. T1w and T2w images underwent quality scoring (0 = no artifacts, 1 = mild artifacts and 2 = severe artifacts) for sharpness, ringing, and contrast-to-noise ratio and QC thresholds applied (pass = 0–0.25, check = 0.5–1, fail = 1.25–2), as detailed previously [7]. Diffusion images were quality checked using the FSL EDDY QC tool [27], which applies non-parametric corrections for motion and distortion and uses Gaussian Process predictions to repair affected slices [28]. Slice-to-volume alignment was performed for intra-volume motion correction [29]. Single-shot sLASER spectra were frequency, phase, and eddy current corrected and then averaged, excluding shots with motion artifacts or unwanted coherences, using MRspa (https://www.cmrr.umn.edu/downloads/mrspa/) [24]. Spectra with poor water suppression, excessive linewidth (> 15 Hz) or those collected from an incorrect VOI were excluded from analysis.

2.5 | MRI Data Availability

MRI data were available from a total of 355 visits and included volumetric and microstructural measurements of the brain, the cerebellum and the brainstem, and neurometabolite levels from the cerebellar white matter and pons. For spectroscopy analyses, total *N*-acetylaspartate (tNAA), myo-inositol (Ins), total Creatine (tCr), and their ratios were of primary interest based on prior work [7, 17].

Structural MRI data were missing for two visits, and three structural datasets were excluded due to segmentation errors after image processing (Figure 1). Diffusion MRI data were missing for five visits; one dataset was excluded due to incorrect field-of-view placement, and four others due to motion artifacts. MRS data were missing for five visits. Additionally, 11 MR spectra from the cerebellar white matter and 32 spectra from the pons were excluded, either due to manual VOI placement errors or broad spectral linewidth.

2.6 | Structural MRI Analysis

Cerebral cortex, subcortical and brainstem volumes were obtained from T1w images segmented with FastSurfer (v2.0.4) [30], a deep-learning platform mirroring FreeSurfer's (v7.3.2) anatomical segmentation [31]. For longitudinal analysis, FreeSurfer's pipeline was applied using an averaged intracranial volume per subject, ensuring consistent within-subject measurements across timepoints [32]. Brainstem subregions (medulla, pons, midbrain, superior cerebellar peduncle) were segmented longitudinally with subject-specific atlases, minimizing processing bias [33]. For brain analysis, 184 structures were extracted (36 subcortical volumes and 148 cortical thickness).

Cerebellar structures were segmented using CerebNet (v1.0.0) [34], a deep-learning method built on the FastSurfer framework, which was trained with MR data from ataxic and non-ataxic individuals [34]. CerebNet employs three independent neural networks for each imaging axis, integrating their outputs to enhance boundary delineation of cerebellar white and gray matter [34]. Thirty different volumes, including 26 individual lobules (without combining left and right), were extracted to assess changes in the cerebellum.

All volumetric MR measures were normalized for intracranial volume estimated by FastSurfer.

2.7 | Diffusion MRI Analysis

Diffusion MRI data were analyzed using the HCP pipeline and FSL DTIFIT (v6.0.4). To minimize bias from differences in *b* values and voxel sizes between Prisma and Skyra platforms, only volumes with $b = 1500\,s/mm^2$ (Prisma) or $b = 1000\,s/mm^2$ (Skyra) were included [35]. Diffusion images were preprocessed for motion, susceptibility, and eddy current distortions using the HCP pipeline [36]. Diffusion tensor metrics (fractional anisotropy, FA; axial diffusivity, AD; radial diffusivity, RD; mean diffusivity, MD) were then computed using DTIFIT (FSL v6.0.4) [37], and FA maps were registered to the Johns Hopkins University (JHU) white matter template [38] with ANTs [39]. The JHU atlas was then projected back into native space to generate 25 standardized ROIs [13]. Skyra-derived diffusivity values were adjusted for *b*-value and voxel size differences using established scaling factors [7]. In total, 100 measures were obtained in this analysis, specifically FA, AD, RD, and MD from 25 ROIs.

2.8 | Magnetic Resonance Spectroscopy Analysis

Spectral data were quantified in LCModel (v6.3.0G) [40] with a simulated metabolite basis set [24]. Metabolite levels were corrected for tissue-specific water T2, water content, and cerebrospinal fluid fraction [10]. Only metabolites with cohort-wide mean Cramér–Rao lower bounds (CRLBs) ≤ 20% were included in the statistical analyses, with exclusions applied for failed fits (CRLB = 999%). Nineteen measures, 10 for cerebellar white matter and 9 for pons, were extracted for analysis.

2.9 | Statistical Analysis

Quantitative variables were expressed as median [Q1; Q3] and qualitative variables as frequency (%). Comparisons between genotypes at baseline were performed using ANOVA, with model assumptions assessed through visual inspection of

residual normality, followed by post hoc pairwise *t*-tests with Holm adjustments for multiple comparisons.

Progression of clinical and MR measures was assessed with linear mixed models, using time since inclusion as the time variable, genotype (Controls, SCA1, SCA3) or ataxia status (Control, Preataxic, Ataxic) and their interaction. Random effects included independent intercept and slope to account for intra-genotype or intra-status variability in rate of progression. We assessed the significance of progression for each ataxic status/genotype across all MR variables. To address the relatively small sample size and high data dimensionality (over 300 MR measures obtained from 3 MR modalities) we first focused on 86 measures hypothesized to be sensitive to longitudinal change based on prior literature (Table S5). For this hypothesis-driven analysis, a significance threshold of $p < 0.01$ was used to mitigate type I error. The hypothesis-driven analysis was followed by an exploratory analysis of the remaining MR variables, where *p*-values were adjusted using the Holm method to account for multiple comparisons. Effect sizes were calculated as the mean annual progression divided by the square root of the sum of the random slope variance and residual variance, consistent with the interpretation of Cohen's *d* for annual progression [41]. Confidence intervals for effect sizes were estimated by bootstrapping over 1000 runs.

Pearson correlations between the rate of progression of the 15 most sensitive MRI measures (i.e., with largest effect sizes across SCAs) and COAs (including all slopes, normalized CAG repeat lengths, baseline SARA scores and NfL levels) were calculated using the individual random slopes estimated from the previously described models. Only participants who were ataxic at baseline or phenoconverted during the study were included to limit the MRI-COA correlation analysis to cases with observable clinical progression. For easier interpretation, the direction of the slopes for MRI measures that decrease over time on average, e.g., regional volumes with progressive atrophy, was inverted for all participants. Hence, a positive slope indicates worsening, e.g., increasing atrophy. Therefore, a positive correlation between two MR measures indicates co-occurring neurodegenerative changes.

For the top three MR metrics, we estimated sample sizes to conduct a trial that aims to slow the rate of progression of the MR outcomes by 30%–100% over one year, with 80% power. Sample sizes were estimated separately for ataxic and preataxic groups, with SARA as reference in the ataxic group, using the linear mixed models and the pooled SD derived from the individual slope variance and the residual error variance.

Statistical tests were performed at the conventional two-tailed type I error of 0.05. Data were analyzed using R version 4.2.0.

3 | Results

3.1 | Cohort Characteristics

The SCA groups were age-, sex-, and handedness-matched to controls at enrollment (Table 1). Both SCA groups were at an early stage at baseline (median SARA < 5) and matched for SARA; 42% of the mutation carriers were at preataxic stage. Preataxic individuals were younger than ataxic individuals, as expected, with no difference between their CAG repeat numbers. NfL levels were higher in both SCA groups than controls, and higher in ataxic than preataxic individuals.

The cohort was followed for a median of three years, during which 1/3 of preataxic individuals phenoconverted, based on a SARA ≥ 3 at one follow-up visit (Table 1). SCA groups remained matched to controls at follow-up (Tables S1–S4).

SARA changed less than one point per year for SCAs and did not change in controls. When the preataxic and ataxic mutation carriers were analyzed separately, SARA did not change in the preataxic group and increased annually by a median of 0.9 points (IQR 0.6–1.5) in the ataxic group.

3.2 | MRI Changes in Control Participants and Participants With Early-Stage SCA

Control participants showed progressive volume loss in the caudate and diffusivity changes in the posterior thalamic radiation, with small effect sizes ($d < 0.4$) (Tables S7 and S9).

To investigate SCA-related MRI changes, we first evaluated subject-level trajectories of MR measures that were previously shown to change over time in SCA1 or SCA3: The pons volume [42] and pontine tNAA/Ins [10], a neuroglial indicator measured by MRS, progressively declined and mean diffusivity (MD) of the middle cerebellar peduncle (MCP) [17] increased in expansion carriers (Figure 2). As expected, participants with higher baseline SARA scores had smaller pons volumes, higher MD of MCP, and lower pontine tNAA/Ins at baseline, consistent with strong cross-sectional correlations between these measures and SARA [7]. Interestingly, however, the progression rates (slopes) seemed consistent between participants with higher versus lower baseline SARA, especially for the pons volume, indicating a constant atrophy rate in this preataxic and early-stage disease. Additionally, greater reliability of the pons volume than that of the diffusion MRI (MD of MCP) and MRS (tNAA/Ins) measures was discernible from the data variation in individual trajectories of both expansion carriers and controls.

Among the 86 MR measures hypothesized to change (Table S5), 36 measures were more sensitive to change than SARA for SCA1 ($d = 0.37$) and 13 measures were more sensitive than SARA for SCA3 ($d = 0.44$) (Tables S6–S14). Volumes of infratentorial structures (pons, brainstem, cerebellar white matter) showed the highest sensitivity to change in both SCAs, with pons volume as the most sensitive measure ($d = 1.3$) (Figure 3). Other measures with moderate-to-high effect sizes ($d \geq 0.5$) included volumes of deep gray matter structures (thalamus, caudate), diffusivities of cerebellar peduncles and MRS measures (tNAA/Ins, tNAA/tCr, Ins). The rate of change of these MR outcomes was significantly higher in SCAs than controls, including those that displayed age-related change in controls, such as the caudate volume.

Among the remaining MR measures (exploratory analysis), enlargement of the third and fourth ventricles and volume loss

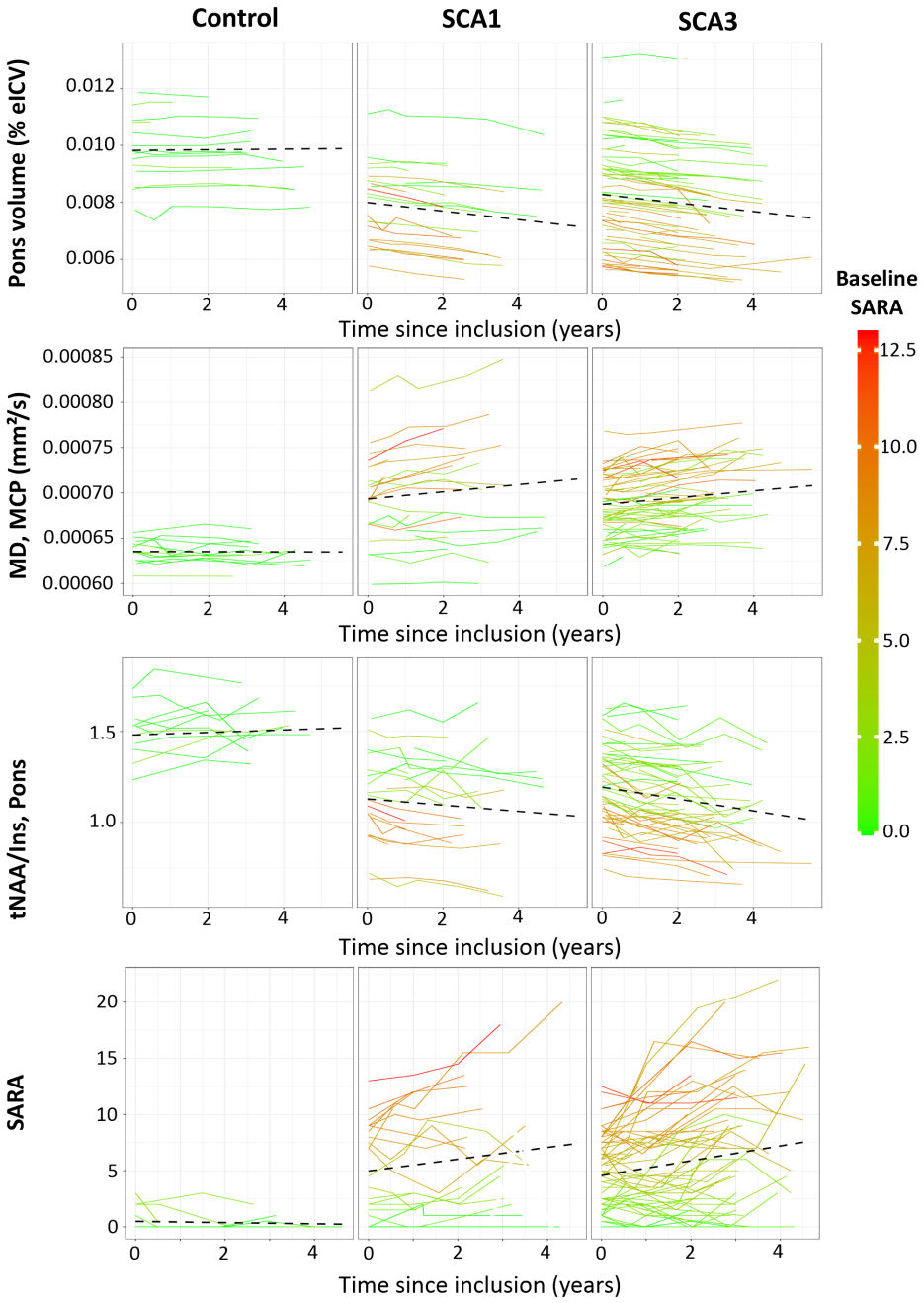

FIGURE 2 | Participant-level trajectories for selected MR outcomes (pons volume expressed as percentage of estimated total intracranial volume, the mean diffusivity (MD) of the middle cerebellar peduncle (MCP) and pontine total *N*-acetylaspartate-to-myo-inositol (tNAA/Ins) ratio) and SARA. Dotted lines represent the mean progression estimated with the linear mixed model.

of the cerebellar cortex and Crus I in both SCAs, lobule VI in SCA1, and ventral diencephalon in SCA3 were more sensitive to change than SARA (Tables S6–S14).

To assess if the most sensitive MR measures differed between genotypes, the slopes and effect sizes of all MR outcomes were compared between SCA1 and SCA3, separately for volumes, cortical thickness, MRS, and diffusion MRI measures (Figure 4A, Tables S6–S14). Effect sizes of MR outcomes were highly correlated between the two SCAs with some exceptions: SCA1 showed faster progression in cerebellar structures, specifically the volume of the anterior lobe and microstructure of the inferior cerebellar peduncles (Tables S6, S9–S12). In addition, changes in metabolite concentrations and ratios were faster in the cerebellar white matter in SCA1, while they were faster in the pons in SCA3 (Tables S13 and S14).

3.3 | MRI Changes in Preataxic and Ataxic Participants

Because the most sensitive MR measures overlapped between the two genotypes, we further analyzed the data as preataxic and ataxic groups combining genotypes. In the preataxic

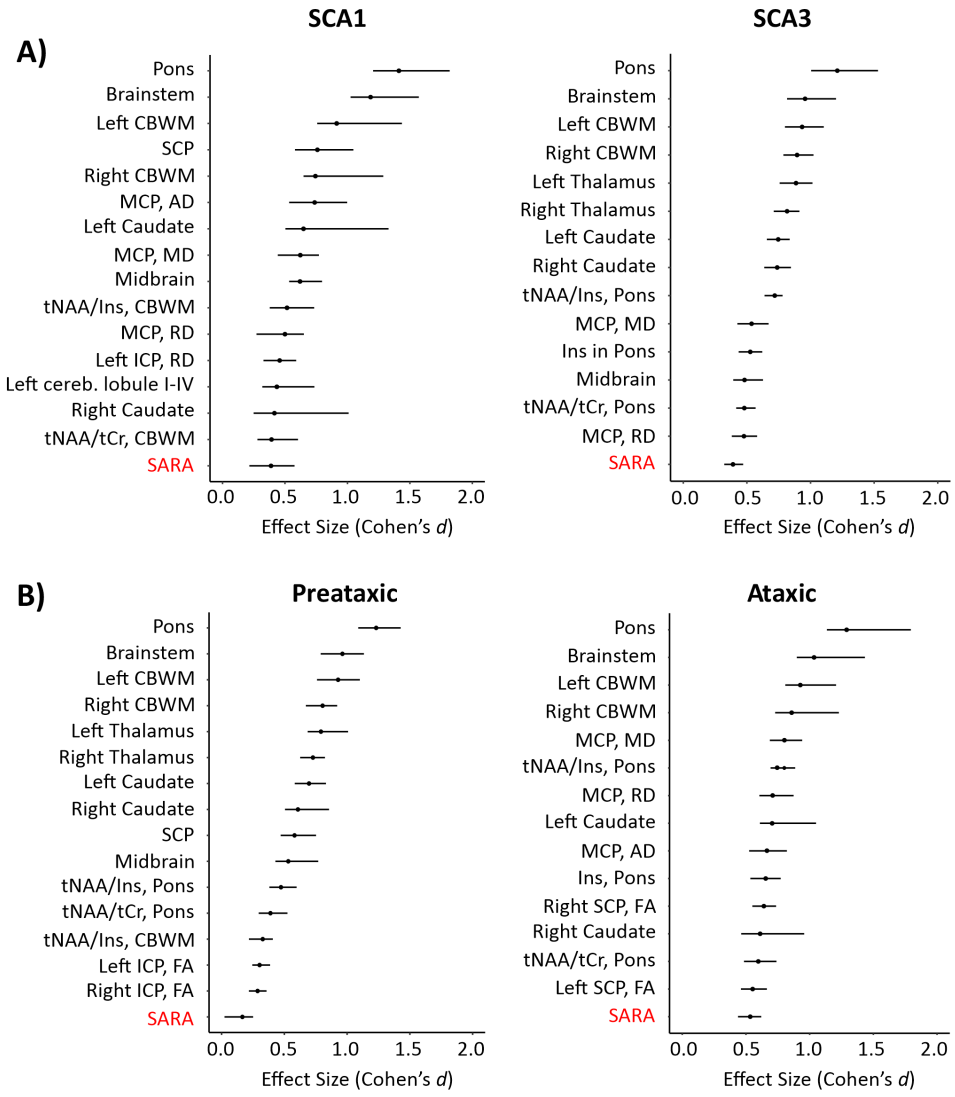

FIGURE 3 | Forest plots showing effect sizes (Cohen's *d*) of the most responsive MR outcomes and SARA change for (A) SCA1 and SCA3 groups and (B) preataxic and ataxic groups. Error bars were computed for each measure using a bootstrapping approach and represent the 95% confidence interval. CBWM, cerebellar white matter; ICP, inferior cerebellar peduncle; MCP, middle cerebellar peduncle; SCP, superior cerebellar peduncle.

group, the volumes of pons, cerebellar white matter, brainstem, midbrain, caudate, thalamus, and superior cerebellar peduncle (SCP) had moderate-to-high effect sizes ($d \geq 0.5$) while the SARA effect size was low ($d = 0.12$) (Figure 4B, Tables S15–S23). In the ataxic group, pons, cerebellar white matter, brainstem, caudate volumes, MCP and SCP diffusion MRI measures, and pontine metabolite levels and ratios outperformed SARA ($d = 0.67$). The pons volume had the highest sensitivity to change in both preataxic ($d = 1.09$) and ataxic ($d = 1.48$) groups. The rate of change of these MR outcomes was significantly higher in preataxic and ataxic groups than controls, except for the caudate volume and MCP diffusivities, which did not differ between preataxic and control groups (Tables S16, S18–S21). MCP diffusivities (MD, radial diffusivity, RD, and axial diffusivity, AD) showed the largest differences in the rate of change between preataxic and ataxic groups (Tables S15–S23).

The exploratory analysis of preataxic and ataxic groups highlighted ventricle enlargement as another sensitive outcome measure. The fourth ventricle volume was the most sensitive outcome in the preataxic ($d = 0.73$) and third ventricle volume in the ataxic group ($d = 0.93$) (Table S16).

3.4 | Clinical Correlations

Three groups of associations were apparent from Pearson correlation analyses between changes in clinical and most sensitive imaging outcomes (Figure 5): Volume changes (pons, brainstem, midbrain, cerebellar white matter and SCP) showed moderate-to-strong correlations between each other ($r = 0.46$–0.98), but were not correlated with clinical change nor baseline characteristics, with one exception: SCP and left cerebellar white matter volumes were negatively associated with SARA change, i.e., participants with faster atrophy in these regions had slower SARA progression (Figure S1). COA changes (SARA, FSS, PHQ9, EQ5D, INAS, FARS-ADL, CCFS) were also correlated with each other ($r = 0.26$–0.70). Lastly, significant associations were present between the slopes of

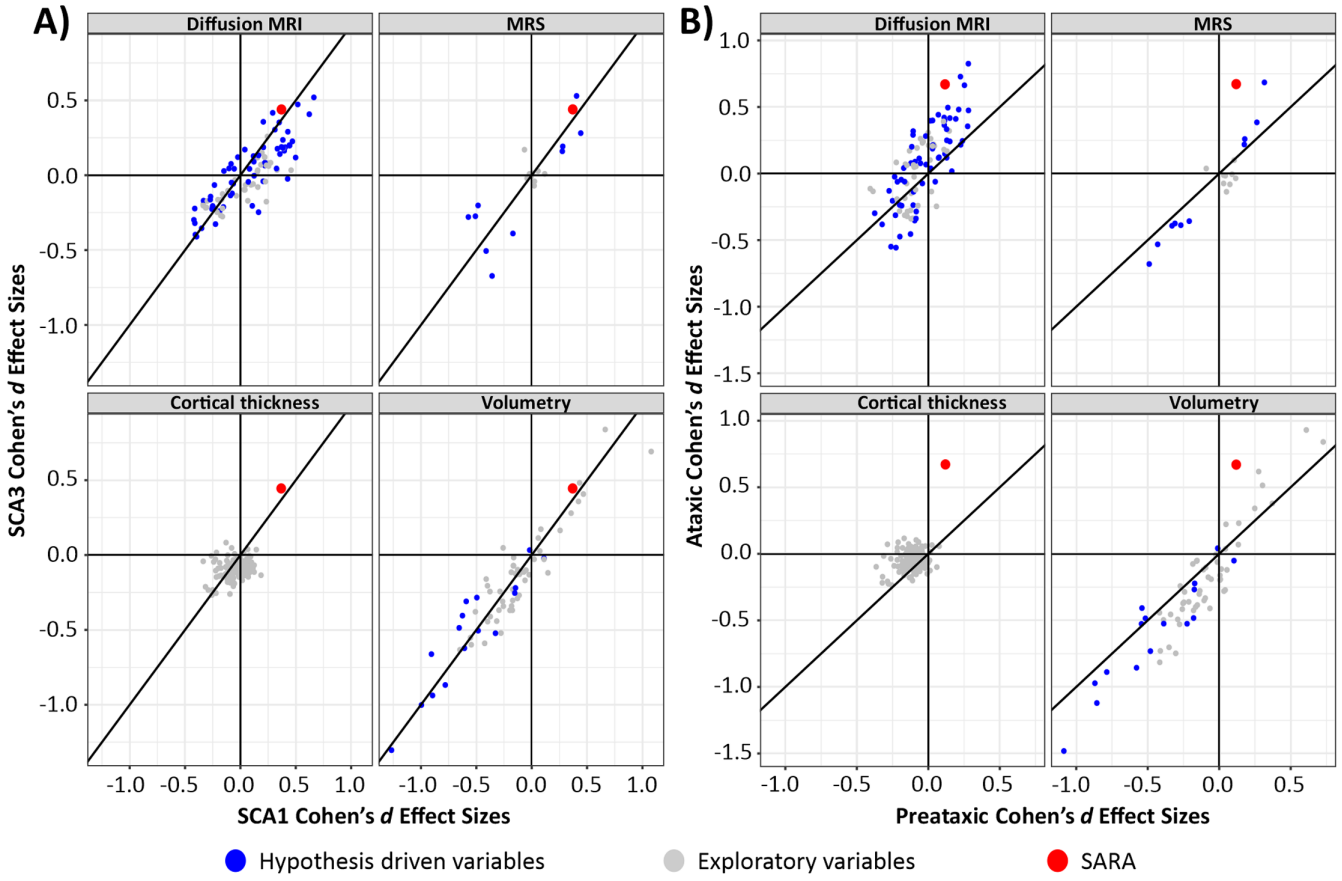

FIGURE 4 | Correlations between Cohen's *d* effect sizes for all diffusion MRI, magnetic resonance spectroscopy (MRS), cortical thickness and volumetry measures between (A) SCA1 and SCA3 groups and (B) preataxic and ataxic groups. Blue data points represent the measures hypothesized to change and the gray data points the exploratory measures. The SARA effect size is represented by a red data point. The solid line indicates the unity line.

select diffusion MRI and MRS outcomes ($r = 0.32–0.51$), and between change in these MR outcomes and COA changes. Specifically, changes in MCP diffusivities and pontine Ins were associated with SARA, CCFS and FARS-ADL change and pontine tNAA/Ins change with FARS-ADL change ($r = 0.28–0.47$).

3.5 | Sample Size Estimation for Interventional Trials

Finally, we estimated sample sizes for preventive and early-stage interventional trials of one-year duration, using the three most sensitive MRI outcomes for both genotypes (Figure 3), and compared them to using SARA as endpoint for an early-interventional trial. We do not report estimates based on the SARA score for a preventive trial, as its minimal change at the preataxic stage would lead to impractically large sample size requirements.

The estimated sample sizes using data from preataxic individuals ranged from 73 (pons) to 150 (left cerebellar white matter) participants per arm to detect a 50% reduction in progression with 80% power in a preventive trial, i.e., an interventional trial at preataxic stage (Figure 6). For an early interventional trial, now including only early-stage symptomatic individuals, the estimated sample size for pons volume was 64 participants per arm, compared to 389 for SARA.

4 | Discussion

This study identified MRI endpoints most sensitive to early pathology progression in two common SCAs using a multimodal MRI protocol in the clinical trial setting. The findings support the feasibility of preventive trials in these SCAs. The combination of longitudinal multimodal MRI measures with a comprehensive clinical characterization of participants provides essential data to design early-stage trials before irreversible neurodegenerative changes in SCA1 and SCA3. This approach can be extended to other hereditary neurodegenerative diseases to establish reliable imaging endpoints in prodromal stages of diseases and to facilitate early-stage clinical trials. Similar longitudinal multimodal MRI data are increasingly available for more prevalent disorders, such as Alzheimer's disease, frontotemporal dementia, and amyotrophic lateral sclerosis [43–45]. The use of a harmonized, state-of-the-art MRI protocol that results in high precision in the extracted MR outcomes is arguably more critical for rare hereditary neurodegenerative diseases with limited sample sizes. These diseases, on the other hand, provide an opportunity to transform neurodegenerative disease management from symptomatic treatment to prevention.

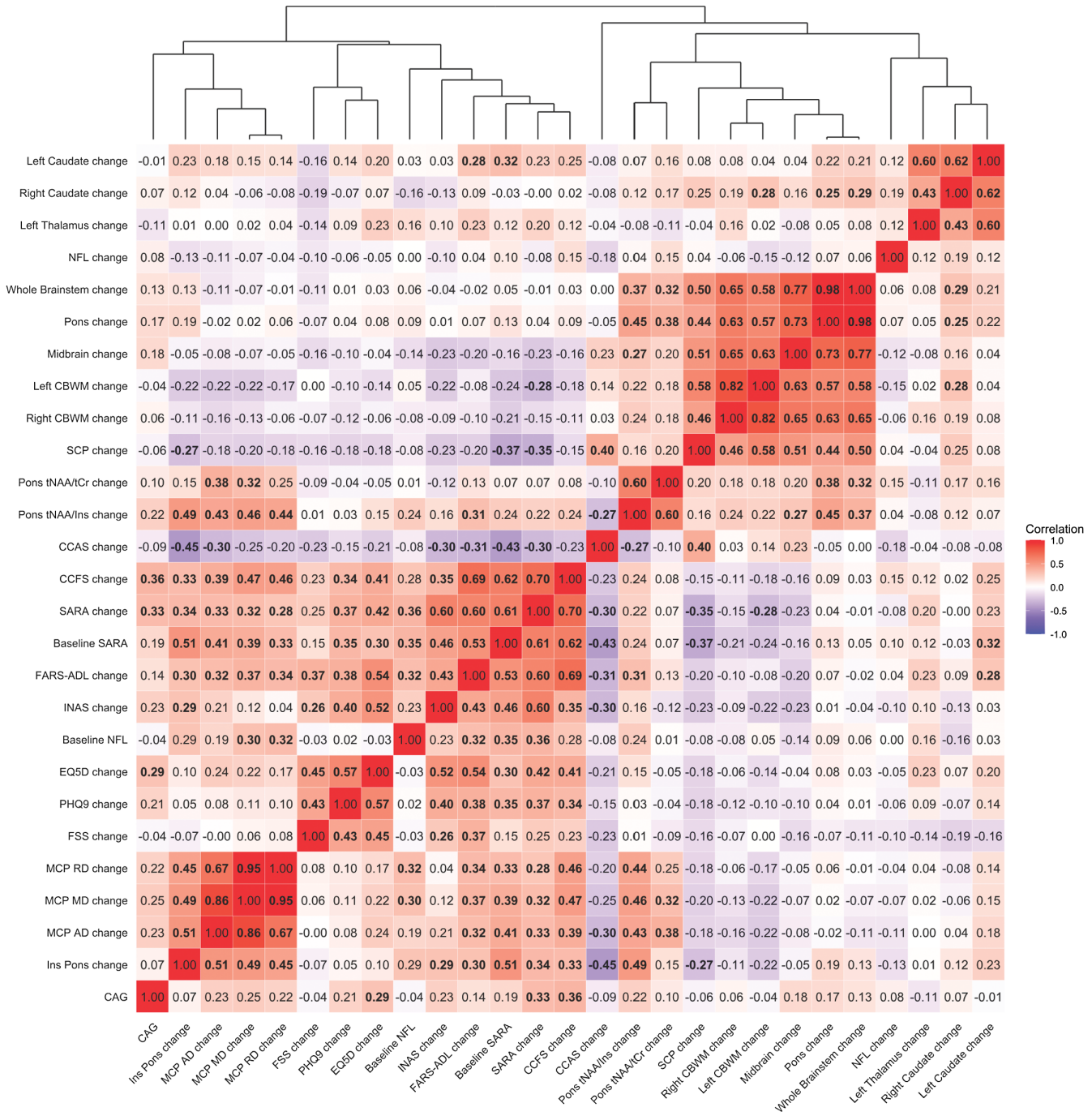

FIGURE 5 | Correlation heatmap between clinical and MRI variable slopes and select baseline measures. Colors reflect correlation coefficients (*r*), with statistically significant values indicated in bold. Hierarchical clustering was used to generate the dendrogram.

The study expands previous efforts to characterize progression of imaging abnormalities in SCA1 and SCA3 [9–11, 14, 42, 46–48], and identifies numerous MR measures that outperform SARA. The poorer effect size of SARA in comparison to MRI measures is related to the greater variability observed in this clinical outcome with marked daily fluctuations. The ataxia research community has been working to address this known limitation of the clinical scales by better understanding the psychometric characteristics of SARA and other COAs [49] and, developing wearable [50] and video-based devices to objectively and precisely assess the ataxia severity [51]. In parallel, validated MRI outcomes are expected to have great value particularly in early-stage trial designs.

We identified pons volume as the most sensitive outcome to pathology progression in preataxic and early SCA1 and SCA3. Pons volume is also highly sensitive in later stages [9, 10, 12, 42, 46–48]. This is advantageous for trial design as regional volumes are derived from 3D T1-weighted MRI, which is widely accessible and provides reproducible metrics through automated MRI processing pipelines [52]. Importantly, basal ganglia and thalamus volumes also showed progressive atrophy before ataxia onset.

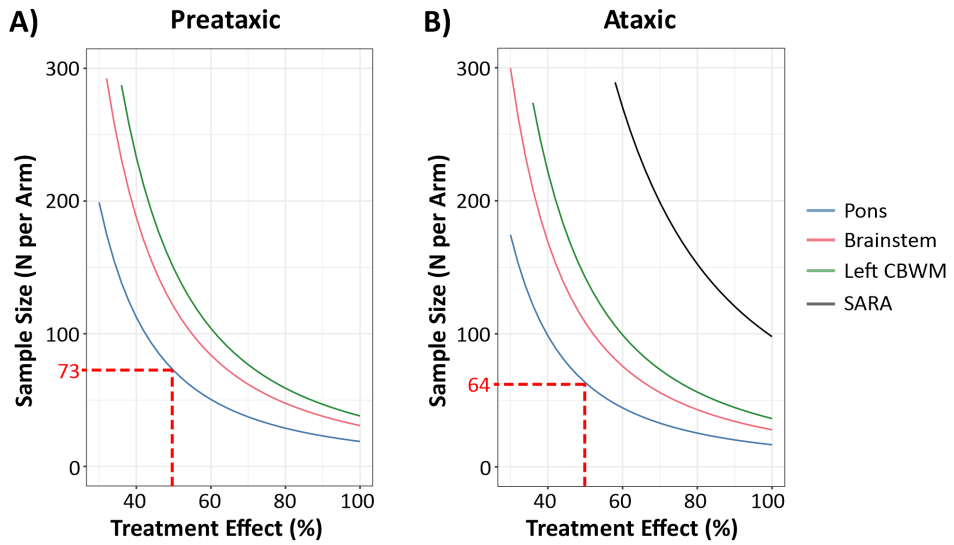

FIGURE 6 | Sample size estimation for a 2-arm (A) preventive trial and (B) early interventional trial of 1-year duration to detect a significant difference in progression between a treated versus placebo group of 30% to 100% using the top three responsive MR metrics, pons, left cerebellar white matter (CBWM) and whole brainstem volume, (B) and SARA as primary outcomes. The sample sizes required for a 50% treatment effect are indicated in red.

In addition to infratentorial and deep gray matter volumes, microstructural and neurochemical measures were sensitive to early progressive pathology, consistent with prior reports at preataxic stage [10, 11, 14, 17], but had lower sensitivity to change than volumetric measures, likely due to greater measurement variability.

These findings support the use of the pons volume as an outcome measure in preventive trials of common SCAs. In addition, a six-fold reduction in sample size is predicted relative to SARA in an early-stage therapeutic trial. We previously predicted a five-fold sample size reduction for a 6-month long trial when using a diffusion MRI-based endpoint compared to SARA based on the 6-month follow-up data in a subset of the READISCA imaging cohort [17]. The longer follow-up and larger sample size in the current study pinpointed the most sensitive MR outcomes and allowed more definitive sample size estimations. Multi-variate analyses may allow further reductions in sample sizes because different MR measures provide complementary information about aspects of pathological changes and their time courses.

Despite the overlap in the most sensitive MRI measures between SCA1 and SCA3, the diffusion MRI and MRS data also indicate a genotype-specific pattern of neurodegeneration, with faster change in the cerebellum in SCA1 and brainstem in SCA3 at this early disease stage. Considering a caudorostral progression in both SCAs, these findings indicate that microstructural and neurochemical changes in SCA1 occur earlier than those in SCA3. Consistently, upper motor signs are present in a larger fraction of preataxic individuals with SCA1 than SCA3 [18].

To validate candidate imaging biomarkers as trial outcomes, their associations with COAs, including PROMs, need to be demonstrated [53]. Pons volume, pontine MRS measurements, and cerebellar peduncle diffusion MRI metrics correlate cross-sectionally with SARA and FARS-ADL [7, 9, 14, 47]. Longitudinally, changes in MCP diffusivity and pontine MRS measures, rather than regional volumes, exhibited significant correlations with SARA and FARS-ADL progression. This is likely due to faster progression of these MR outcomes in ataxic than preataxic stages. Interestingly, SCP atrophy, which was the most sensitive structural measure to detect preataxic abnormalities cross-sectionally in both SCAs [7], decelerated with ataxia onset, resulting in a negative correlation with SARA.

At this very early stage in the pathology progression, the atrophy rates of the most sensitive volumetric MR measures (pons, brainstem and cerebellar white matter) were not associated with SARA progression, unlike the microstructural metrics and neurometabolite levels. This indicates that the microstructural and neurochemical measures, rather than the loss of tissue, are more closely associated with the functional outcomes, namely the cerebellar ataxic phenotype, at this early disease stage. These measures also show more genotype-specificity, consistent with their close association with disease-specific pathology. On the other hand, literature evidence points to the predictive value of volumetric measures. Thus, a prior single-site study reported that baseline pons volume predicts subsequent SARA progression in SCA1 [47]. Similarly, a multisite study showed that lower medulla oblongata volume predicts future SARA progression in SCA3 [14]. Another single site study showed that one-year change in pontine volume correlated with subsequent change in ataxia severity and gait in a later stage cohort [54]. Therefore, the lack of an association between the progression rates of the top volumetric measures and SARA at this early stage does not mean the volume measurements are not associated with meaningful clinical change across the disease continuum. Further longitudinal data from large, multisite cohorts are needed to confirm the predictive value of the MRI outcomes and for refining models that estimate disease progression and time to onset in preataxic individuals [14].

Interestingly, the rate of NfL increase also did not correlate with the rate of atrophy at this early disease stage, indicating that NfL and the structural MRI outcomes reflect different aspects of the pathology progression in these two SCAs. NfL levels are known to increase very early in the disease course but progress little during the symptomatic progression, as was recently shown for a large SCA3 cohort [14]. On the other hand, the volumetric measures progress continuously.

The primary limitation of this study is the relatively small sample size for SCA1 compared to SCA3, although the SCA1-to-SCA3 ratio aligns with their relative prevalence [1]. Consequently, effect size estimates for SCA1 are less reliable than those for SCA3. While the preataxic and ataxic group analyses combined the genotypes here, trials for disease modifying, e.g., gene silencing, therapies will be disease-specific. The small number of phenoconverters with each genotype did not allow identification of genotype-specific MRI measures that predict the transition from the preataxic to ataxic stage. In the larger READISCA cohort ($N = 222$), 17 preataxic participants phenoconverted (5 SCA1 and 12 SCA3); these individuals displayed higher levels of NfL at baseline [55]. Phenoconverters with either genotype and available MRI data ($N = 11$, 3 SCA1 and 8 SCA3) had higher levels of cerebellar white matter atrophy at baseline. Furthermore, higher total creatine in the cerebellar white matter at baseline was predictive of faster SARA progression [55]. Further assessments of preataxic READISCA participants who have not phenoconverted yet, as well as combining phenoconversion data across multiple imaging cohorts is expected to provide sufficient sample sizes for robust predictive analyses. Finally, all MRI data in the READISCA study were acquired using Siemens scanners. However, the most sensitive MRI outcomes were regional volumes that can be reproducibly measured across platforms.

In summary, structural, microstructural, and neurochemical measures are highly sensitive to pathology progression in preataxic and early stages for common SCAs. Pons volume may enable the inclusion of preataxic individuals in clinical trials, making preventive SCA trials feasible. Changes in select microstructural and neurochemical measures display genotype specificity and parallel changes in clinical and patient-reported outcomes.

Author Contributions

T.J.R.R., E.P., and G.Ö. directly accessed and verified the data. G.Ö., T.A., A.D., T.K., H.P., S.T.d.M., and C.L. conceptualized and designed the study. T.J.R.R., E.P., Y.W.P., S.T.d.M., J.M.J., M.P., G.B., P.E., J.F., C.U.O., P.B.B., J.D.S., E.-M.R., S.H.S., T.H.M., K.O.B., H.P., T.K., A.D., T.A., C.L., and G.Ö. contributed to the acquisition and analysis of data. T.J.R.R. and G.Ö. drafted the manuscript with help from E.P. All authors contributed to data interpretation, reviewed and edited the final manuscript, had access to raw data, and had final responsibility for the decision to submit for publication. In addition, members of the READISCA Consortium contributed to the collection of clinical data (Table S24).

Acknowledgments

The READISCA investigators would like to thank all participants for their enduring willingness and interest in this research. We extend gratitude to Dr. Dinesh Deelchand for assistance with MR protocol development, Brian Hanna for translating the defacing/de-identification pipeline to a Docker container, Diane Hutter, Ann Fishman, Jason Macmore, Brigitte Jacoby, Samantha Pierce, Jessica Magenheim, Anke Ruehling, and Hortense Hurmic for study coordination, and Chantel Potvin and Erika Espinoza for project management.

Funding

This work was supported by the National Institute of Neurological Disorders and Stroke (NINDS) grant U01 NS104326 and Biogen Inc. The Center for Magnetic Resonance Research is supported by the National Institute of Biomedical Imaging and Bioengineering (NIBIB) grant P41 EB027061, the NINDS Institutional Center Cores for Advanced Neuroimaging award P30 NS076408 and S10 OD017974. Research reported in this publication was also supported by an Academic Investment Research Program (AIRP) award at the University of Minnesota and the National Center for Advancing Translational Sciences of the National Institutes of Health Award Number UL1TR000114. A portion of this work was performed in the McKnight Brain Institute of the University of Florida at the National High Magnetic Field Laboratory's Advanced Magnetic Resonance Imaging and Spectroscopy (AMRIS) Facility, which is supported by National Science Foundation Cooperative Agreement DMR-1644779 and the State of Florida and was supported in part by an NIH award, S10 OD021726, for High End Instrumentation. This research was completed while Young Woo Park, Ph.D. was a staff researcher at the Center for Magnetic Resonance Research at the University of Minnesota. The content is solely the responsibility of the authors and does not necessarily represent the official views of the National Institutes of Health, the Henry M. Jackson Foundation for the Advancement of Military Medicine Inc., the Uniformed Services University of the Health Sciences (USUHS), the Department of Defense (DoD), or the Departments of the Army, Navy, or Air Force.

Conflicts of Interest

Dr. Thiago J.R. Rezende receives funding from the National Institute of Health (NIH), Friedreich's Ataxia Research Alliance (FARA), Biogen, and PTC therapeutics. Dr. Gülin Öz receives funding from the NIH, Biogen, National Ataxia Foundation (NAF), and has consulted for IXICO Technologies Limited, uniQure biopharma B.V., VICO Therapeutics, Servier, Sanofi, and UCB Biopharma SRL/Lacerta Therapeutics Inc. and serves on the Scientific Advisory Board of BrainSpec Inc. Dr. Chiadi U. Onyike receives research support from the NIH, NAF, Association for Frontotemporal Degeneration, Alector Inc., and Denali Pharmaceuticals. He also consulted for the Lewy Body Association, Alector, AviadoBio, Eli Lilly, Otsuka, Neuvivo, Reata, and Sanofi. Dr. Eva-Maria Ratai receives funding from the NIH, National Science Foundation (NSF), and Research Foundation for The SUNY Stony Brook University, Baszucki Brain Research Fund, serves on the Scientific Advisory Board of BrainSpec Inc., and is a consultant for Alethia Biotherapeutics. Dr. Sophie Tezenas du Montcel receives research support from Biogen and has consulted for VICO Therapeutics. Dr. Jeremy D. Schmahmann discloses that he is the inventor of the CCAS/Schmahmann Scale, the PROM-Ataxia, Brief Ataxia Rating Scale, and Cerebellar Neuropsychiatric Rating Scale to which the General Hospital Corporation holds the copyright. He consults for Biohaven, received support from Biohaven and the National Ataxia Foundation for the development of the PROM-Ataxia, is site PI for Biohaven NCT03952806 and NCT03701399, and receives royalties from Elsevier, MacKeith, Oxford, and Springer. Dr. Khalaf O. Bushara receives funding from the Bob Allison Ataxia Research Foundation. Dr. Tetsuo Ashizawa receives funding from the NIH, Biogen, and NAF. Dr. Thomas Klockgether is receiving research support from the Bundesministerium für Bildung und Forschung (BMBF), the NIH, and Servier. Within the last 24 months, he has received consulting fees from UCB and Vico Therapeutics. Dr. Jennifer Faber was funded within the Advanced Clinician Scientist Programme (ACCENT, funding code 01EO2107), by the German Federal Ministry of Education and Research (BMBF), the National

Ataxia Foundation (NAF), and as a PI of the iBehave Network, sponsored by the Ministry of Culture and Science of the State of North Rhine-Westphalia, and received consultancy honoraria from Vico therapeutics and Biogen, unrelated to the present manuscript. Dr. Jennifer Faber is a member of the European Reference Network for Rare Neurological Diseases. Dr. Sub H. Subramony receives funding from the Food and Drug Administration (FDA), Muscular Dystrophy Association (MDA), FARA, and NAF, and has consulted for Reata, Biogen, Avidity, Arrowhead, Amicus, Fulcrum, Solid Biosciences, and PTC. Dr. Alexandra Durr is currently receiving grants from the NIH, Foundation de la Recherche Médicale (FRM), Brain-Team, and ANR. Paris Brain Institute receives consulting fees on Dr. Alexandra Durr's behalf from Biogen, AskBIo, Servier, UCB, Genome Quebec, and HuntIX. She holds partly Patent B 06291873.5 "Anaplerotic therapy of Huntington's disease and other polyglutamine diseases." Dr. Christophe Lenglet receives funding from the NIH, FDA, Department of Defense of the USA, FARA, NAF, and Biogen. Dr. Jonathan M. DuBois and Dr. H. Moore Arnold were employed by and held stock in Biogen during the conduct of this research. Dr. James M. Joers receives support from FARA and NIH.

Data Availability Statement

Deidentified participant-level clinical and imaging data from READISCA and a data dictionary defining each field in the set will be available from the National Institute of Mental Health Data Archive (https://nda.nih.gov/, Collection C3155) to investigators researching neurodegenerative diseases in accordance with the General Data Protection Regulation after the publication of the manuscript. Data requests can also be sent to the Corresponding Author.

References

1. T. Klockgether, C. Mariotti, and H. L. Paulson, "Spinocerebellar Ataxia," *Nature Reviews. Disease Primers* 5, no. 1 (2019): 24.

2. T. Ashizawa, G. Oz, and H. L. Paulson, "Spinocerebellar Ataxias: Prospects and Challenges for Therapy Development," *Nature Reviews Neurology* 14, no. 10 (2018): 590–605.

3. G. Coarelli, M. Coutelier, and A. Durr, "Autosomal Dominant Cerebellar Ataxias: New Genes and Progress Towards Treatments," *Lancet Neurology* 22, no. 8 (2023): 735–749.

4. T. Schmitz-Hubsch, S. T. du Montcel, L. Baliko, et al., "Scale for the Assessment and Rating of Ataxia: Development of a New Clinical Scale," *Neurology* 66, no. 11 (2006): 1717–1720.

5. R. J. Bateman, T. L. Benzinger, S. Berry, et al., "The DIAN-TU Next Generation Alzheimer's Prevention Trial: Adaptive Design and Disease Progression Model," *Alzheimers Dement* 13, no. 1 (2017): 8–19.

6. M. Benatar, J. Wuu, P. M. Andersen, et al., "Design of a Randomized, Placebo-Controlled, Phase 3 Trial of Tofersen Initiated in Clinically Presymptomatic SOD1 Variant Carriers: The ATLAS Study," *Neurotherapeutics* 19, no. 4 (2022): 1248–1258.

7. J. Chandrasekaran, E. Petit, Y. W. Park, et al., "Clinically Meaningful Magnetic Resonance Endpoints Sensitive to Preataxic Spinocerebellar Ataxia Types 1 and 3," *Annals of Neurology* 93, no. 4 (2023): 686–701.

8. J. M. Joers, D. K. Deelchand, T. Lyu, et al., "Neurochemical Abnormalities in Premanifest and Early Spinocerebellar Ataxias," *Annals of Neurology* 83, no. 4 (2018): 816–829.

9. I. M. Adanyeguh, V. Perlbarg, P. G. Henry, et al., "Autosomal Dominant Cerebellar Ataxias: Imaging Biomarkers With High Effect Sizes," *NeuroImage: Clinical* 19 (2018): 858–867.

10. D. K. Deelchand, J. M. Joers, A. Ravishankar, et al., "Sensitivity of Volumetric Magnetic Resonance Imaging and Magnetic Resonance Spectroscopy to Progression of Spinocerebellar Ataxia Type 1," *Movement Disorders Clinical Practice* 6, no. 7 (2019): 549–558.

11. C. M. de Oliveira, V. B. Leotti, S. Polita, et al., "The Longitudinal Progression of MRI Changes in Pre-Ataxic Carriers of SCA3/MJD," *Journal of Neurology* 270, no. 9 (2023): 4276–4287.

12. A. Nigri, L. Sarro, A. Mongelli, et al., "Spinocerebellar Ataxia Type 1: One-Year Longitudinal Study to Identify Clinical and MRI Measures of Disease Progression in Patients and Presymptomatic Carriers," *Cerebellum* 21, no. 1 (2022): 133–144.

13. Y. W. Park, J. M. Joers, B. Guo, et al., "Assessment of Cerebral and Cerebellar White Matter Microstructure in Spinocerebellar Ataxias 1, 2, 3, and 6 Using Diffusion MRI," *Frontiers in Neurology* 11 (2020): 411.

14. M. Berger, H. Garcia-Moreno, M. Ferreira, et al., "Progression of Biological Markers in Spinocerebellar Ataxia Type 3: Longitudinal Analysis of Prospective Data From the ESMI Cohort," *Lancet Regional Health* 55 (2025): 101339.

15. M. Pandolfo, K. Reetz, A. Darling, et al., "Efficacy and Safety of Leriglitazone in Patients With Friedreich Ataxia: A Phase 2 Double-Blind, Randomized Controlled Trial (FRAMES)," *Neurology Genetics* 8, no. 6 (2022): e200034.

16. S. Budd Haeberlein, P. S. Aisen, F. Barkhof, et al., "Two Randomized Phase 3 Studies of Aducanumab in Early Alzheimer's Disease," *Journal of Prevention of Alzheimer's Disease* 9, no. 2 (2022): 197–210.

17. T. J. R. Rezende, E. Petit, Y. W. Park, et al., "Sensitivity of Advanced Magnetic Resonance Imaging to Progression Over Six Months in Early Spinocerebellar Ataxia," *Movement Disorders* 39, no. 10 (2024): 1856–1867.

18. S. Tezenas du Montcel, E. Petit, T. Olubajo, et al., "Baseline Clinical and Blood Biomarkers in Patients With Preataxic and Early-Stage Disease Spinocerebellar Ataxia 1 and 3," *Neurology* 100, no. 17 (2023): e1836–e1848.

19. R. P. Maas, J. van Gaalen, T. Klockgether, and B. van de Warrenburg, "The Preclinical Stage of Spinocerebellar Ataxias," *Neurology* 85, no. 1 (2015): 96–103.

20. M. P. Harms, L. H. Somerville, B. M. Ances, et al., "Extending the Human Connectome Project Across Ages: Imaging Protocols for the Lifespan Development and Aging Projects," *NeuroImage* 183 (2018): 972–984.

21. D. K. Deelchand, A. Berrington, R. Noeske, et al., "Across-Vendor Standardization of Semi-LASER for Single-Voxel MRS at 3T," *NMR in Biomedicine* 34, no. 5 (2021): e4218.

22. D. K. Deelchand, P. G. Henry, J. M. Joers, et al., "Plug-and-Play Advanced Magnetic Resonance Spectroscopy," *Magnetic Resonance in Medicine* 87, no. 6 (2022): 2613–2620.

23. Y. W. Park, D. K. Deelchand, J. M. Joers, et al., "AutoVOI: Real-Time Automatic Prescription of Volume-of-Interest for Single Voxel Spectroscopy," *Magnetic Resonance in Medicine* 80, no. 5 (2018): 1787–1798.

24. D. K. Deelchand, I. M. Adanyeguh, U. E. Emir, et al., "Two-Site Reproducibility of Cerebellar and Brainstem Neurochemical Profiles With Short-Echo, Single-Voxel MRS at 3T," *Magnetic Resonance in Medicine* 73, no. 5 (2015): 1718–1725.

25. K. A. Archie and D. S. Marcus, "DicomBrowser: Software for Viewing and Modifying DICOM Metadata," *Journal of Digital Imaging* 25, no. 5 (2012): 635–645.

26. M. Milchenko and D. Marcus, "Obscuring Surface Anatomy in Volumetric Imaging Data," *Neuroinformatics* 11, no. 1 (2013): 65–75.

27. M. Bastiani, M. Cottaar, S. P. Fitzgibbon, et al., "Automated Quality Control for Within and Between Studies Diffusion MRI Data Using a Non-Parametric Framework for Movement and Distortion Correction," *NeuroImage* 184 (2019): 801–812.

28. J. L. R. Andersson and S. N. Sotiropoulos, "An Integrated Approach to Correction for Off-Resonance Effects and Subject Movement in Diffusion MR Imaging," *NeuroImage* 125 (2016): 1063–1078.

29. J. L. R. Andersson, M. S. Graham, I. Drobnjak, H. Zhang, N. Filippini, and M. Bastiani, "Towards a Comprehensive Framework for Movement and Distortion Correction of Diffusion MR Images: Within Volume Movement," *NeuroImage* 152 (2017): 450–466.

30. L. Henschel, D. Kugler, and M. Reuter, "FastSurferVINN: Building Resolution-Independence Into Deep Learning Segmentation Methods—A Solution for HighRes Brain MRI," *NeuroImage* 251 (2022): 118933.

31. B. Fischl, D. H. Salat, A. J. van der Kouwe, et al., "Sequence-Independent Segmentation of Magnetic Resonance Images," *NeuroImage* 23, no. Suppl 1 (2004): S69–S84.

32. M. Reuter, N. J. Schmansky, H. D. Rosas, and B. Fischl, "Within-Subject Template Estimation for Unbiased Longitudinal Image Analysis," *NeuroImage* 61, no. 4 (2012): 1402–1418.

33. J. E. Iglesias, K. Van Leemput, P. Bhatt, et al., "Bayesian Segmentation of Brainstem Structures in MRI," *NeuroImage* 113 (2015): 184–195.

34. J. Faber, D. Kugler, E. Bahrami, et al., "CerebNet: A Fast and Reliable Deep-Learning Pipeline for Detailed Cerebellum Sub-Segmentation," *NeuroImage* 264 (2022): 119703.

35. N. D. Papinutto, F. Maule, and J. Jovicich, "Reproducibility and Biases in High Field Brain Diffusion MRI: An Evaluation of Acquisition and Analysis Variables," *Magnetic Resonance Imaging* 31, no. 6 (2013): 827–839.

36. M. F. Glasser, S. N. Sotiropoulos, J. A. Wilson, et al., "The Minimal Preprocessing Pipelines for the Human Connectome Project," *NeuroImage* 80 (2013): 105–124.

37. T. E. Behrens, M. W. Woolrich, M. Jenkinson, et al., "Characterization and Propagation of Uncertainty in Diffusion-Weighted MR Imaging," *Magnetic Resonance in Medicine* 50, no. 5 (2003): 1077–1088.

38. K. Hua, J. Zhang, S. Wakana, et al., "Tract Probability Maps in Stereotaxic Spaces: Analyses of White Matter Anatomy and Tract-Specific Quantification," *NeuroImage* 39, no. 1 (2008): 336–347.

39. B. B. Avants, N. J. Tustison, G. Song, P. A. Cook, A. Klein, and J. C. Gee, "A Reproducible Evaluation of ANTs Similarity Metric Performance in Brain Image Registration," *NeuroImage* 54, no. 3 (2011): 2033–2044.

40. S. W. Provencher, "Estimation of Metabolite Concentrations From Localized In Vivo Proton NMR Spectra," *Magnetic Resonance in Medicine* 30, no. 6 (1993): 672–679.

41. M. Brysbaert and M. Stevens, "Power Analysis and Effect Size in Mixed Effects Models: A Tutorial," *Journal of Cognition* 1, no. 1 (2018): 9.

42. K. Reetz, A. S. Costa, S. Mirzazade, et al., "Genotype-Specific Patterns of Atrophy Progression Are More Sensitive Than Clinical Decline in SCA1, SCA3 and SCA6," *Brain* 136, no. Pt 3 (2013): 905–917.

43. A. Arani, B. Borowski, J. Felmlee, et al., "Design and Validation of the ADNI MR Protocol," *Alzheimer's & Dementia* 20, no. 9 (2024): 6615–6621.

44. H. K. van der Burgh, H. J. Westeneng, R. Walhout, et al., "Multimodal Longitudinal Study of Structural Brain Involvement in Amyotrophic Lateral Sclerosis," *Neurology* 94, no. 24 (2020): e2592–e2604.

45. A. M. Staffaroni, P. A. Ljubenkov, J. Kornak, et al., "Longitudinal Multimodal Imaging and Clinical Endpoints for Frontotemporal Dementia Clinical Trials," *Brain* 142, no. 2 (2019): 443–459.

46. C. C. Piccinin, T. J. R. Rezende, J. L. R. de Paiva, et al., "A 5-Year Longitudinal Clinical and Magnetic Resonance Imaging Study in Spinocerebellar Ataxia Type 3," *Movement Disorders* 35, no. 9 (2020): 1679–1684.

47. T. H. van Prooije, K. C. J. Kapteijns, J. J. A. van Asten, et al., "Multimodal, Longitudinal Profiling of SCA1 Identifies Predictors of Disease Severity and Progression," *Annals of Neurology* 96, no. 4 (2024): 774–787.

48. K. C. J. Kapteijns, T. H. van Prooije, H. Li, et al., "The Pattern and Dynamics of White Matter Alterations in Spinocerebellar Ataxia Type 1: A Diffusion-Weighted Magnetic Resonance Imaging Study," *NeuroImage. Clinical* 46 (2025): 103783.

49. S. C. Milne, A. Murphy, N. Georgiou-Karistianis, E. M. Yiu, M. B. Delatycki, and L. A. Corben, "Psychometric Properties of Outcome Measures Evaluating Decline in Gait in Cerebellar Ataxia: A Systematic Review," *Gait & Posture* 61 (2018): 149–162.

50. V. V. Shah, R. Rodriguez-Labrada, F. B. Horak, et al., "Gait Variability in Spinocerebellar Ataxia Assessed Using Wearable Inertial Sensors," *Movement Disorders* 36, no. 12 (2021): 2922–2931.

51. M. Grobe-Einsler, A. Taheri Amin, J. Faber, et al., "Development of SARA^{home}, a New Video-Based Tool for the Assessment of Ataxia at Home," *Movement Disorders* 36, no. 5 (2021): 1242–1246.

52. J. Jovicich, M. Marizzoni, R. Sala-Llonch, et al., "Brain Morphometry Reproducibility in Multi-Center 3T MRI Studies: A Comparison of Cross-Sectional and Longitudinal Segmentations," *NeuroImage* 83 (2013): 472–484.

53. T. Klockgether, T. Ashizawa, B. Brais, et al., "Paving the Way Toward Meaningful Trials in Ataxias: An Ataxia Global Initiative Perspective," *Movement Disorders* 37, no. 6 (2022): 1125–1130.

54. T. H. van Prooije, K. C. J. Kapteijns, J. J. A. van Asten, M. M. Verbeek, T. W. J. Scheenen, and B. P. van de Warrenburg, "The Predictive Validity of Pontine Volume Change in Spinocerebellar Ataxia Type 1 (SCA1)," *Neurobiology of Disease* 215 (2025): 107078.

55. E. Petit, G. Coarelli, D. Morgan, et al., "Predictive Models for Ataxia Progression and Conversion in Spinocerebellar Ataxia Type 1 and 3," *Brain* (2025), https://doi.org/10.1093/brain/awaf408.

Supporting Information

Additional supporting information can be found online in the Supporting Information section. **Figure S1:** Scatterplots of participant-level slopes are shown for selected clinical (SARA and FARS-ADL) and MR outcomes (pons (s_Pons) and superior cerebellar peduncle (s_SCP) volumes with both expressed as percentage of estimated total intracranial volume, the mean diffusivity (MD) of the middle cerebellar peduncle (MCP) and pontine total *N*-acetylaspartate-to-myo-inositol (tNAA/Ins) ratio). Pearson correlation coefficients (*r*) are shown in the top half of the association matrix. **Table S1:** Cohort characteristics at visit 2. **Table S2:** Cohort characteristics at visit 3. **Table S3:** Cohort characteristics at visit 4. **Table S4:** Cohort characteristics at visit 5. **Table S5:** Regions and neurochemicals known to be affected in SCA1 and SCA3 and used in the hypothesis driven analysis. **Table S6:** Longitudinal changes (slopes) in cerebellar volumes in controls, SCA1 and SCA3. **Table S7:** Longitudinal changes (slopes) in FastSurfer/FreeSurfer volumes in controls, SCA1 and SCA3. **Table S8:** Longitudinal changes (slopes) in FastSurfer/FreeSurfer cortical thickness in controls, SCA1 and SCA3. **Table S9:** Longitudinal changes (slopes) in regional axial diffusivities in controls, SCA1 and SCA3. **Table S10:** Longitudinal changes (slopes) in regional fractional anisotropy in controls, SCA1 and SCA3. **Table S11:** Longitudinal changes (slopes) in regional mean diffusivities in controls, SCA1 and SCA3. **Table S12:** Longitudinal changes (slopes) in regional radial diffusivities in controls, SCA1 and SCA3. **Table S13:** Longitudinal changes (slopes) in cerebellar white matter (CBWM) neurometabolites in controls, SCA1 and SCA3. **Table S14:** Longitudinal changes (slopes) in pontine neurometabolites in controls, SCA1 and SCA3. **Table S15:** Longitudinal changes (slopes) in cerebellar volumes in controls, preataxic and ataxic cohorts. **Table S16:** Longitudinal changes (slopes) in FastSurfer/FreeSurfer volumes in controls, preataxic and ataxic cohorts. **Table S17:** Longitudinal changes (slopes) in FastSurfer/FreeSurfer cortical thickness in controls, preataxic and ataxic cohorts. **Table S18:** Longitudinal changes (slopes) in regional axial diffusivities in controls, preataxic and ataxic cohorts. **Table S19:** Longitudinal changes (slopes) in regional fractional anisotropy in controls, preataxic and ataxic cohorts.

Table S20: Longitudinal changes (slopes) in regional mean diffusivities in controls, preataxic and ataxic cohorts. **Table S21:** Longitudinal changes (slopes) in regional radial diffusivities in controls, preataxic and ataxic cohorts. **Table S22:** Longitudinal changes (slopes) in cerebellar white matter (CBWM) neurometabolites in controls, preataxic and ataxic cohorts. **Table S23:** Longitudinal changes (slopes) in pontine neurometabolites in controls, preataxic and ataxic cohorts. **Table S24:** READISCA consortium collaborators that contributed to the collection of clinical data.